

A critical point in $\text{Sr}_{2-x}\text{IrO}_4$ and less distorted IrO_6 octahedra induced by deep Sr-vacancies

Jie Cheng^{a*}, Shengli Liu^{a,b*}, Bin Li^{a*}, Haiyun Wang^a, Yu Wang^c and Wei Xu^{d,e}

^a College of Science, Center of Advanced Functional Ceramics, Nanjing University of Posts and Telecommunications, Nanjing, Jiangsu 210023, China

^b Nanjing University (Suzhou) High-Tech Institute, Suzhou, 215123, China

^c Shanghai Synchrotron Radiation Facility, Shanghai Institute of Applied Physics, Chinese Academy of Sciences, Shanghai 201204, China

^d Beijing Synchrotron Radiation Facility, Institute of High Energy Physics, Chinese Academy of Sciences, Beijing 100049, China

^e Rome International Center for Materials Science, Superstripes, RICMASS, via dei Sabelli 119A, I-00185 Roma, Italy

E-mail: chengj@njupt.edu.cn, liusl@njupt.edu.cn and libin@njupt.edu.cn

Abstract

For the $\text{Sr}_{2-x}\text{IrO}_4$ system, recent work pointed out the abnormal electronic and magnetic properties around a critical point. Here, to understand Sr-vacancy effect on spin-orbit coupled Mott insulator Sr_2IrO_4 , the electronic structure and local structure distortion for $\text{Sr}_{2-x}\text{IrO}_4$ system have been investigated by x-ray absorption spectroscopy (XAS). By comparing the intensity of white-line features at the Ir $L_{2,3}$ -edge x-ray absorption near-edge spectroscopy (XANES), we observe a sudden rise of the branching ratio in the vicinity of the critical point. Further analysis on the Ir L_3 -edge extended x-ray absorption fine structure (EXAFS) and calculated data demonstrated that the abrupt enhancement of the branching ratio is intimately related

to the less distorted IrO_6 octahedra induced by deep Sr-vacancies, which in turn alters the relatively strength of the spin-orbit coupling (SOC) and crystal electric field (CEF) that would dictate the abnormal behavior of electronic and magnetic structure near the critical point.

Keywords: Sr_2IrO_4 ; x-ray absorption spectroscopy; a critical point; local structure

1. Introduction

The $5d$ transition metal oxides (TMOs) have been the topic of intense research in recent years due to their numerous intriguing phenomena [1, 2]. Because of the large atomic mass associated with $5d$ elements, the strong relativistic spin-orbit coupling (SOC) effect is an important consideration in describing the physical properties of $5d$ TMOs, and it rigorously competes with other relevant energies, particularly the on-site Coulomb repulsion U and crystal electric field (CEF) interactions arising from the surrounding coordinate environment [3]. Consequently, a variety of exotic quantum phases, including the $J_{eff}=1/2$ Mott state [1, 2], superconductivity [4, 5], a topological insulator [6, 7], Weyl semimetal with Fermi arcs [8], are shown and expected in $5d$ TMOs.

In the case of the most well-known $5d$ TMOs, the layered Sr_2IrO_4 known as SOC-related Mott insulator, has been subjected to the most extensive investigations due to its structural and electronic similarities to those of the celebrated La_2CuO_4 [9]. Sr_2IrO_4 , which has the K_2NiF_4 structure, is based on Ir^{4+} in IrO_6 octahedra [10]. The octahedral CEF splits the $5d$ bands into t_{2g} and e_g states, and the t_{2g} manifold splits into two effective angular momentum energy levels (a doublet $J_{eff} = 1/2$ and a quartet $J_{eff} = 3/2$) via the strong SOC [1, 2]. Since the Ir^{4+} ions provide five $5d$ -electrons, four of them fill the lower $J_{eff} = 3/2$ bands, and one electron partially fills the $J_{eff} = 1/2$ band where the Fermi level E_F resides. The $J_{eff} = 1/2$ band is so narrow that even a reduced U is sufficient to open a gap, supporting an insulating behavior [1, 2]. Accordingly, the delicate competition among the various interactions such as the CEF,

SOC and U plays a crucial role in realizing the $J_{eff} = 1/2$ intriguing physics for Sr_2IrO_4 .

Several theoretical investigations predicted that the unconventional high-temperature superconductivity can be induced by carrier doping in this Sr_2IrO_4 -based system [4, 11-13]. Very recently, experiments on doped Sr_2IrO_4 have uncovered tantalizing evidence of a Fermi surface split up into disconnected segments (“Fermi arcs”) [14] and a low-temperature gap with d-wave symmetry [15, 16], which are hallmarks of the doped cuprates [17]. However, the true sense of superconductivity has not been found yet, regardless of the electron and hole-doping.

As is known to all, material properties are in a close relationship with their atomic structure. Several reports pointed out that carrier doping can alter lattice parameters and further change the electronic and magnetic behaviors of Sr_2IrO_4 [18-21]. Thus, one of the important issues to be resolved for Sr_2IrO_4 -based system is how carrier doping affect their physical properties in terms of local atomic structure. For instance, Bhatti *et al.* established a relationship between temperature dependent magnetic property and the structural parameters by means of x-ray diffraction (XRD) measurement on Sr_2IrO_4 [22]. Furthermore, our pervious investigations suggest the synergistic effect of regular IrO_6 octahedra and electron doping that accounts for the transition from a Mott insulator to a conductive state in $\text{Sr}_{2-x}\text{La}_x\text{IrO}_4$ -based system [23]. A more accurate and systematic investigation of local atomic displacements induced by carrier doping is still necessary to better understand the Sr_2IrO_4 system, that may be beneficial to uncover the potential superconductivity in SOC-related Mott

insulators.

Synchrotron-radiation-based X-ray absorption spectroscopy (XAS) is a well-recognized local experimental technique capable of giving substantial information (*i.e.* local atomic and electronic structure) for a material [24, 25]. Moreover, Ir $L_{2,3}$ -edge XAS can be competent for providing other valuable information (*e.g.* the strength of SOC) in Ir-based systems [26]. Here, we take the polycrystalline compounds of $\text{Sr}_{2-x}\text{IrO}_4$ as the object of our research. As the Sr-vacancies approach $x \sim 0.45$, the properties of the material change suddenly in three aspects [27]: 1) an insulator-metal transition; 2) a sudden drop of the localization temperature and the antiferromagnetic transition temperature, together with an anomalous sign reverse of the Curie-Weiss temperature; 3) a significant structural change probed by both XRD and Raman spectra. All these aspects strongly suggest the existence of a critical point around $x \sim 0.45$ in this system. Therefore, an investigation of the critical point is highly desired and might be a key to achieve the potential superconductivity in Sr_2IrO_4 -based system. In this contribution, detailed investigations of the Sr-vacancy effect at the critical point are probed by a comprehensive analysis of Ir $L_{2,3}$ -edge XAS.

2. Experiments and Calculations

Polycrystalline compounds with nominal compositions of $\text{Sr}_{2-x}\text{IrO}_4$ were synthesized by solid-state reaction method as mentioned elsewhere [27]. The samples were well characterized for their phase purity prior to the XAS measurements. We collected both the Ir L_2 -edge x-ray absorption near edge structure (XANES) and L_3 -edge extended x-ray absorption fine structure (EXAFS) spectra of $\text{Sr}_{2-x}\text{IrO}_4$ at

room temperature, which occur at energy of 12.824keV and 11.215keV, respectively. The XAS spectra were collected at the BL-14W1 beamline of Shanghai Synchrotron Radiation Facility (SSRF). Several scans were collected to ensure the spectral reproducibility. The storage ring was working at electron energy of 3.5 GeV, and the maximum stored current was about 250mA. The energy of the incident energy was tuned by scanning a Si (111) double crystal monochromator with energy resolution about 10^{-4} . Data reduction was performed using the IFEFFIT program package [28].

Density functional theory (DFT) calculations for $\text{Sr}_{2-x}\text{IrO}_4$ system were carried out within the local-density approximation (LDA) including SOC and on-site Coulomb U using OPENMX [29], based on the linear-combination-of-pseudo-atomic-orbitals (LCPAO) method [30]. SOC is treated *via* a fully relativistic j -dependent pseudopotential in the non-collinear DFT scheme, with 300 Ry of energy cutoff and $11 \times 11 \times 11$ k-grid. For $\text{Sr}_{2-x}\text{IrO}_4$, only one and two of the eight Sr atoms were removed in a unit cell, which correspond to $x = 0.25$ and 0.5, respectively. Atomic positions of the structure have been relaxed until all the force components became smaller than 10^{-4} eV/a.u. The on-site Coulomb interaction parameter U is set to 2.0 eV for Ir d -orbitals in our LDA + SOC + U calculations.

3. Results and Discussions

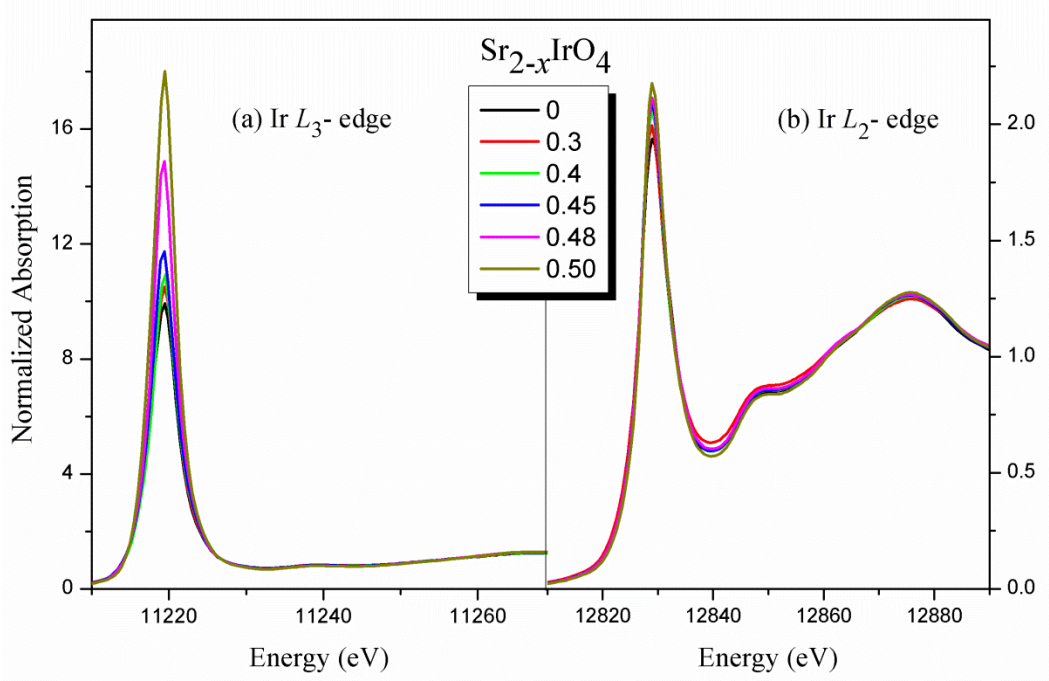


Fig. 1. Ir $L_{2,3}$ -edge normalized XANES spectra of $\text{Sr}_{2-x}\text{IrO}_4$.

The Ir $L_{2,3}$ -edge XANES spectra of $\text{Sr}_{2-x}\text{IrO}_4$ compounds are provided in Fig. 1. The most striking characteristic is the prominent white-line (WL) features which correspond to $2p \rightarrow 5d$ electronic transitions. From the dipole selection rules, ΔJ must be equal to 0 or ± 1 , it follows that for Sr_2IrO_4 -based system the Ir L_2 -edge will be sensitive to transitions involving $5d_{3/2}$ (*i.e.* $J_{\text{eff}} = 3/2$) holes, while the L_3 -edge will be related to both $5d_{5/2}$ (upper Hubbard band associated with $J_{\text{eff}} = 1/2$ and the CEF e_g manifolds) and $5d_{3/2}$ final states. Because the WL features are more pronounced at the L_3 edge than the L_2 edge, we can also infer that these unoccupied $5d$ states are primarily $5d_{5/2}$ rather than $5d_{3/2}$ in nature, consistent with the almost completely filled $J_{\text{eff}} = 3/2$ bands in Sr_2IrO_4 [2]. Furthermore, the integrated intensity of the WL features is proportional to the local density of unoccupied final states (*i.e.* the population of $5d$ holes) in the system. From Fig. 1 the integrated intensity of WL features at both

absorption edges grows steadily with increasing the Sr-vacancies, pointing out the increment of Ir-5d holes in $\text{Sr}_{2-x}\text{IrO}_4$ compounds. To demonstrate the above discussion, the DFT calculations for $\text{Sr}_{2-x}\text{IrO}_4$ ($x = 0, 0.25$ and 0.5) were performed. In Table 1, we summarized the number of electrons for each element. It is found that the holes induced by Sr-vacancies are located around all atoms, especially the Ir atoms, in agreement with the result of XANES spectra.

Table 1

The number of electrons belonging to each atomic species for $\text{Sr}_{2-x}\text{IrO}_4$.

$\text{Sr}_{2-x}\text{IrO}_4$	Ir	Sr	O
$x = 0$	15.91	8.46	6.54
$x = 0.25$	15.84	8.42	6.51
$x = 0.5$	15.52	8.38	6.48

The relative strength of the WL features at the L_3 and L_2 edges (also known as the branching ratio $\text{BR} = I_{L_3}/I_{L_2}$) is an important quantity [26], since it is directly related to the expectation value of the angular part of the SOC of 5d states *via* $\text{BR} = (2+r)/(1-r)$, where $r = \langle \mathbf{L} \cdot \mathbf{S} \rangle / n_h$ and n_h is the average number of 5d holes [31, 32]. For a system with negligible SOC the statistical branching ratio from XANES is 2. To discuss the branching ratio on a quantitative level, the integrated intensity of WL feature at each edge was provided based on the least-squares method as mentioned elsewhere, using a Lorentzian + arctangent fit function [23]. By analysing the XANES spectra, the branching ratio for Sr_2IrO_4 is $\text{BR} = 6.45$, a value which is several

times larger than the statistical one, indicating the presence of extremely large SOC effects. Using $n_h = 5$ we obtain $\langle \mathbf{L} \cdot \mathbf{S} \rangle = 2.99$ in units of \hbar^2 , consistent with other reports [26].

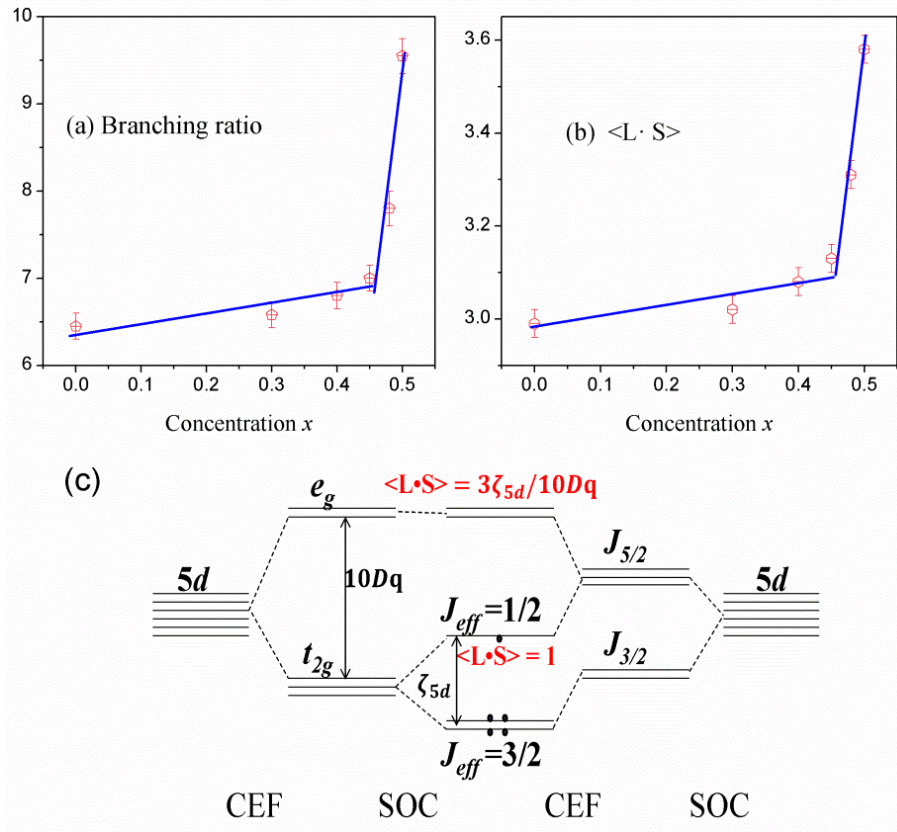


Fig. 2. The branching ratio I_{L_3}/I_{L_2} (a) and $\langle \mathbf{L} \cdot \mathbf{S} \rangle$ (b) as a function of Sr-vacancy concentrations. (c) A schematic energy diagram of 5d level splittings by the CEF and SOC, based on Ref. 2.

As shown in Fig. 2, both the branching ratio and $\langle \mathbf{L} \cdot \mathbf{S} \rangle$ increase gradually with the increasing Sr-vacancies, while a sudden rise occurs in the deep doping region around $x = 0.45$. This anomalous kink reminds us about the critical point in $\text{Sr}_{2-x}\text{IrO}_4$ system, implying potential changes of the fundamental local atomic structure at the critical point. The $\langle \mathbf{L} \cdot \mathbf{S} \rangle$ is a property of the local moment, it is mostly determined by the

SOC and the CEF acting on $5d$ electrons. Note that since XANES probes all empty $5d$ states, the measured $\langle \mathbf{L} \cdot \mathbf{S} \rangle$ will be the sum of two contributions (illustrated in Fig. 2(c)): a single hole in the $J_{eff} = 1/2$ state ($\langle \mathbf{L} \cdot \mathbf{S} \rangle = 1$) and four holes in the e_g -derived states ($\langle \mathbf{L} \cdot \mathbf{S} \rangle = 4 \times 3\zeta_{5d}/10Dq$) [33, 34], where ζ_{5d} represents the SOC of the $5d$ states and $10Dq$ is the parameter of octahedral CEF. Therefore, the Sr-vacancies can effectively alter the relative strength of the SOC and CEF, which could be useful to describe the fundamental properties of $\text{Sr}_{2-x}\text{IrO}_4$ system.

It is well known that Ir atoms play a significant role in extremely strong SOC effects of Sr_2IrO_4 -based system, while the cation substitutions can change the strength of SOC [35]. For instance, a substitution of Ir with Ru/Rh would tune the SOC strength from the strong $5d$ regime to the moderate $4d$ regime [35]. On the other hand, the substitution at Sr sites (*e.g.* La-doping) just tunes the band filling, and does not alter the SOC strength [35]. That is to say, only the substitution at Ir sites can significantly tune the SOC strength of the system. Roughly speaking, in our study Sr-vacancies impose negligible effect on the SOC strength, and we neglect the SOC changes in our discussion. Thus we will focus on the CEF effect *versus* Sr-vacancies.

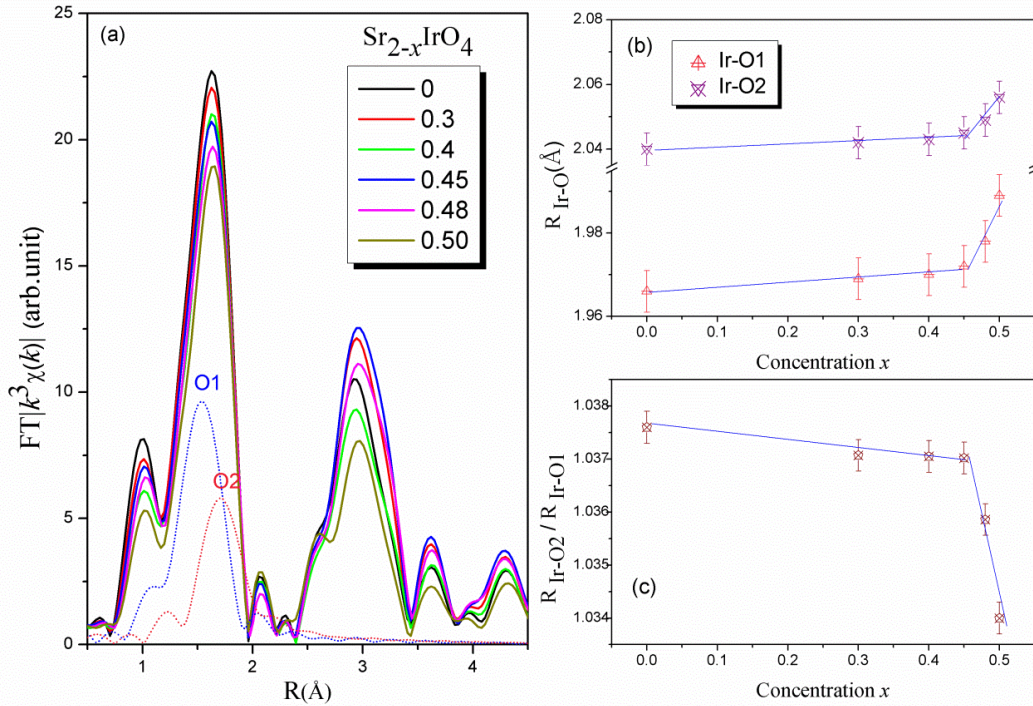


Fig. 3. (a) Fourier transform magnitudes of $k^3\chi(k)$ EXAFS signals of $Sr_{2-x}IrO_4$ compounds at Ir L_3 -edge and the contributions of Ir-O1/O2 pairs calculated by FEFF code. The Results from the fit of Ir-O1/Ir-O2 bond distances are shown in panel (b). (c) The derived differences between the distances of Ir-O1 and Ir-O2 bonds as a function of Sr-vacancy concentrations. Error bars correlated to the uncertainty value are given.

In the Sr_2IrO_4 -based system, the CEF interaction is arisen from surrounding six oxygen atoms in a nearly octahedral local coordinate environment [10]. The IrO_6 octahedron contains two distinct oxygen positions (four basal O1 and two apical O2), which is slightly elongated apically. Therefore, to gain an insight into the local atomic displacements induced by Sr-vacancies, we have undertaken detailed structural study (*e.g.* the bond distances of Ir-O1 and Ir-O2) by means of the Ir L_3 -edge EXAFS spectra. The Fourier transform (FT) magnitudes of the EXAFS oscillations providing real space information around Ir atoms are plotted in Fig. 3(a). Note that the positions

of the peaks in the FT are shifted a few tenths of Å from the actual interatomic distances because of the EXAFS phase shift [36]. Obviously, large changes in the FTs of Ir L_3 -edge can be seen, indicating the atomic displacements induced by Sr-vacancies.

The EXAFS amplitude depends on several factors and is given by the following general equation [37]:

$$\chi(k) = \sum_j \frac{N_j S_0^2}{k R_j^2} f_j(k, R_j) \exp[-2k^2 \sigma_j^2] \exp\left[\frac{-2R_j}{\lambda}\right] \sin[2kR_j + \delta_j(k)] \quad (1)$$

where N_j is the number of neighboring atoms at a distance R_j , S_0^2 is the passive electron reduction factor, $f_j(k, R_j)$ is the backscattering amplitude, λ is the photoelectron mean free path, $\delta_j(k)$ is the phase shift and σ_j^2 is the correlated Debye-Waller factor.

In order to obtain quantitative results, we fit the first peak of EXAFS spectra ($R = 1.0 \sim 2.2$ Å) involving contributions of four basal O1 and two apical O2, which were isolated from the FTs with a rectangular window. The range in k space was $3 \sim 15$ Å⁻¹ and that in R space was $1.0 \sim 2.2$ Å. For the least-squares fits, average structure measured by diffraction on Sr₂IrO₄ system is used as the starting model [27]. The backscattering amplitudes and phase shift were calculated using the FEFF code [38]. Only the radial distances R_j and the corresponding σ_j^2 were allowed to vary, with coordination numbers N_j fixed to the nominal values. The passive electrons reduction factor S_0^2 and photoelectron energy zero E_0 were also fixed after fit trials on different scans. The number of independent parameters which could be determined by EXAFS is limited by the number of the independent data points $N_{\text{ind}} \sim (2\Delta k \Delta R)/\pi$,

where Δk and ΔR are respectively the ranges of the fit in the k and R space [37]. In our case, N_{ind} is 9 ($\Delta k = 12 \text{ \AA}^{-1}$, $\Delta R = 1.2 \text{ \AA}$), sufficient to obtain all parameters.

As shown in Fig. 3(b), the distances of both Ir-O1 and Ir-O2 pairs increase gradually with the increasing Sr-vacancies, while an obvious kink occurs in the deep doping region. Note that the IrO_6 octahedron is slightly elongated apically, and deep Sr-vacancies suddenly decrease the ratio of apical Ir-O2 to basal Ir-O1 distance (illustrated in Fig. 3(c)), indicating less distorted IrO_6 octahedra induced by deep Sr-vacancies. Surprisingly, all these structural changes are in coincidence with the existence of the critical point around $x = 0.45$. That is to say, the changes of fundamental atomic structure would be important to describe the properties around the critical point.

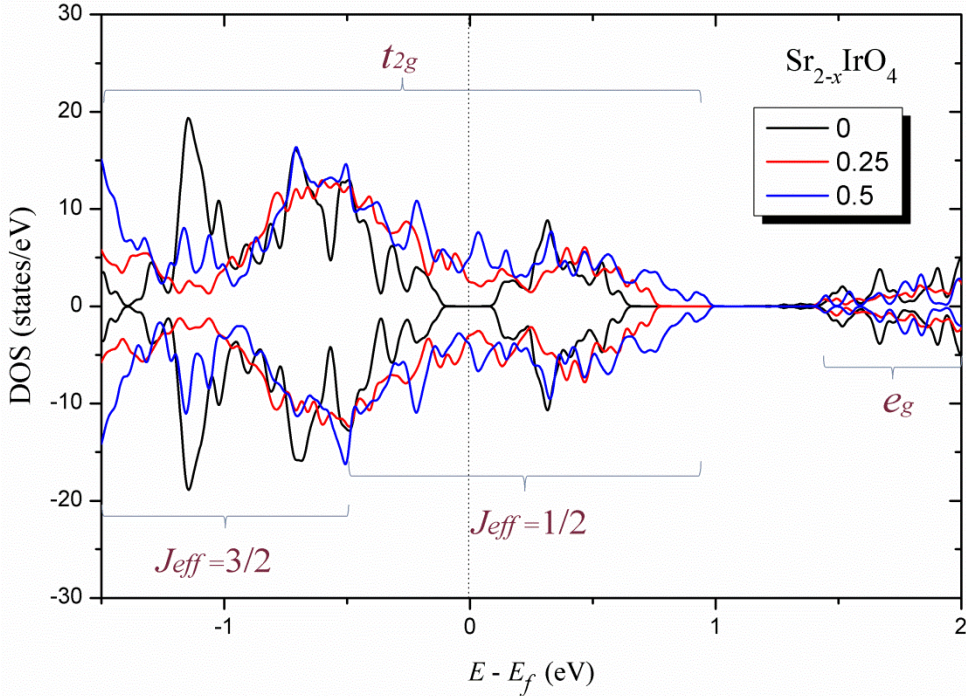


Fig. 4. Total density of states for $\text{Sr}_{2-x}\text{IrO}_4$ system.

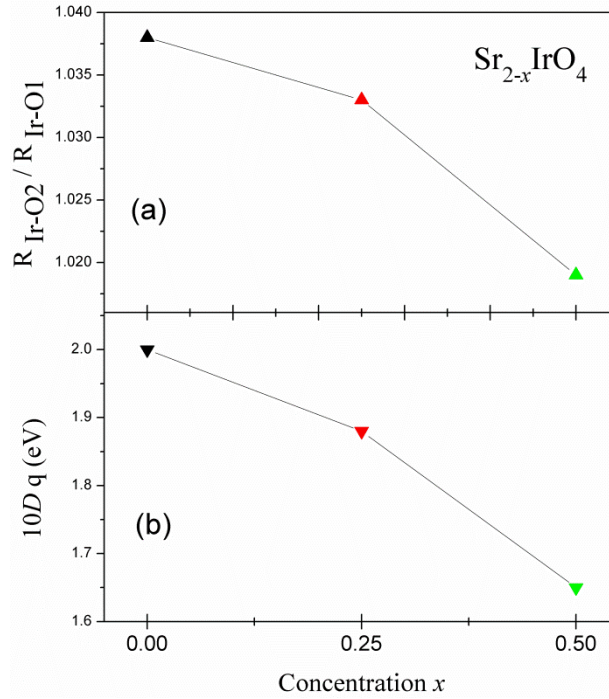


Fig. 5. The ratio of apical Ir-O2 to basal Ir-O1 bond length (a) and the CEF parameter $10Dq$ (b) for $\text{Sr}_{2-x}\text{IrO}_4$ system.

In order to validate the above XAS results, we performed DFT calculations on $\text{Sr}_{2-x}\text{IrO}_4$ system. The total density of states in Fig. 4 suggests that deep Sr-vacancies turn the $\text{Sr}_{2-x}\text{IrO}_4$ system from a Mott insulator to the metallic state, in agreement with the experimental results [27]. As shown in Fig. 5, Sr-vacancies also induce structural changes driving the ratio of apical Ir-O2 to basal Ir-O1 bond length towards the value of 1, suggesting the less distorted IrO_6 octahedra. Accordingly, the $10Dq$ parameter decreases suddenly (*i.e.* the weakened CEF) along with the deep Sr-vacancies, consistent with the abrupt enhancement of $\langle L \cdot S \rangle$.

As mentioned above, our results provide experimental and calculated data on the less distorted IrO_6 octahedra induced by deep Sr-vacancies; this in turn tunes the relatively strength of the SOC and CEF for $\text{Sr}_{2-x}\text{IrO}_4$ system, which would dictate the

abnormal behavior of electronic and magnetic properties at the critical point.

4. Conclusion

To summarize, we have investigated the Sr-vacancy effect on the spin-orbit coupled Sr_2IrO_4 probed by Ir $L_{2,3}$ -edge XAS. By fitting the white line features of Ir $L_{2,3}$ -edge XANES, the sudden enhancement of both the branching ratio and the derived $\langle L\cdot S \rangle$ were observed in the vicinity of the critical point. Further investigations in terms of local structure showed that the abrupt rise of $\langle L\cdot S \rangle$ near the critical point is intimately related to the less distorted IrO_6 octahedra (*i.e.* the weakened CEF). So in this contribution we establish the delicate interplay between the critical point and the regular configuration of IrO_6 octahedra, hoping this point of view could be beneficial to our understanding of abnormal physics properties in $\text{Sr}_{2-x}\text{IrO}_4$ -based system.

Acknowledgement

This work was partly supported by the National Natural Science Foundation of China (NSFC 11405089 and 11504182), the “Six Talents Peak” Foundation of Jiangsu Province (2014-XCL-015), the Nanotechnology Foundation of Suzhou Bureau of Science and Technology (ZXG201444).

References

- [1] B.J. Kim, H. Ohsumi, T. Komesu, S. Sakai, T. Morita, H. Takagi, T. Arima, Phase-Sensitive Observation of a Spin-Orbital Mott State in Sr_2IrO_4 , *Science* 323 (2009) 1329.
- [2] B.J. Kim, H. Jin, S.J. Moon, J.Y. Kim, B.G. Park, C.S. Leem, J. Yu, T.W. Noh, C. Kim, S.J. Oh, J.H. Park, V. Durairaj, G. Cao, E. Rotenberg, Novel $J_{\text{eff}}=1/2$ Mott State Induced by Relativistic Spin-Orbit Coupling in Sr_2IrO_4 , *Phys. Rev. Lett.* 101 (2008) 076402.
- [3] D. Pesin, L. Balents, Mott physics and band topology in materials with strong spin-orbit interaction, *Nature Phys.* 6 (2010) 376.
- [4] F. Wang, T. Senthil, Twisted Hubbard Model for Sr_2IrO_4 : Magnetism and Possible High Temperature Superconductivity, *Phys. Rev. Lett.* 106 (2011) 136402.
- [5] Y.Z. You, I. Kimchi, A. Vishwanath, Doping a spin-orbit Mott insulator: Topological superconductivity from the Kitaev-Heisenberg model and possible application to $(\text{Na}_2/\text{Li}_2)\text{IrO}_3$, *Phys. Rev. B* 86 (2012) 085145.
- [6] A. Shitade, H. Katsura, J. Kunes, X.L. Qi, S.C. Zhang, N. Nagaosa, Quantum Spin Hall effect in a Transition Metal Oxide Na_2IrO_3 , *Phys. Rev. Lett.* 102 (2009) 256403.
- [7] C.H. Kim, H.S. Kim, H. Jeong, H. Jin, J. Yu, Topological Quantum Phase Transition in 5d Transition Metal Oxide Na_2IrO_3 , *Phys. Rev. Lett.* 108 (2012) 106401.
- [8] X.G. Wan, A.M. Turner, A. Vishwanath, S.Y. Savrasov, Topological semimetal and Fermi-arc surface states in the electronic structure of pyrochlore iridates, *Phys. Rev. B* 83 (2011) 205101.
- [9] J. Kim, D. Casa, M.H. Upton, T. Gog, Y.J. Kim, J.F. Mitchell, M. van Veenendaal, M. Daghofer, J. van den Brink, G. Khaliullin, B.J. Kim, Magnetic Excitation Spectra of Sr_2IrO_4 Probed by Resonant Inelastic X-Ray Scattering: Establishing Links to Cuprate Superconductors, *Phys. Rev. Lett.* 108 (2012) 177003.
- [10] M.K. Crawford, M.A. Subramanian, R.L. Harlow, Structure and magnetic studies of Sr_2IrO_4 , *Phys. Rev. B* 49 (1994) 9198.
- [11] H. Watanabe, T. Shirakawa, S. Yunoki, Monte Carlo Study of an Unconventional Superconducting Phase in Iridium Oxide $J_{\text{eff}}=1/2$ Mott Insulators Induced by Carrier Doping, *Phys. Rev. Lett.* 110 (2013) 027002.
- [12] Y. Yang, W.S. Wang, J.G. Liu, H. Chen, J.H. Dai, Q.H. Wang, Superconductivity in doped Sr_2IrO_4 : A functional renormalization group study, *Phys. Rev. B* 89 (2014) 094518.
- [13] Z.Y. Meng, Y.B. Kim, H.Y. Kee, Odd-Parity Triplet Superconducting Phase in Multiorbital Materials with a Strong Spin-Orbit Coupling: Application to Doped Sr_2IrO_4 , *Phys. Rev. Lett.* 113 (2014) 177003.
- [14] Y.K. Kim, O. Krupin, J.D. Denlinger, A. Bostwick, E. Rotenberg, Q. Zhao, J.F. Mitchell, J.W. Allen, B.J. Kim, Fermi arcs in a doped pseudospin-1/2 Heisenberg antiferromagnet, *Science* 345 (2014) 187.
- [15] Y.J. Yan, M.Q. Ren, H.C. Xu, B.P. Xie, R. Tao, H.Y. Choi, N. Lee, Y.J. Choi, T. Zhang, D.L. Feng, Electron-Doped Sr_2IrO_4 : An Analogue of Hole-Doped Superconductors Demonstrated by Scanning Tunneling Microscopy, *Phys. Rev. X* 5 (2015) 041018.
- [16] Y.K. Kim, N.H. Sung, J.D. Denlinger, B.J. Kim, Observation of a d -wave gap in electron-doped Sr_2IrO_4 , *Nature Phys.* 12 (2016) 37.
- [17] B. Keimer, S.A. Kivelson, M.R. Norman, S. Uchida, J. Zaanen, From quantum matter to

- high-temperature superconductivity in copper oxides, *Nature* 518 (2015) 179.
- [18] J.P. Clancy, A. Lupascu, H. Gretarsson, Z. Islam, Y.F. Hu, D. Casa, C.S. Nelson, S.C. LaMarra, G. Cao, Y.J. Kim, Dilute magnetism and spin-orbital percolation effects in $\text{Sr}_2\text{Ir}_{1-x}\text{Rh}_x\text{O}_4$, *Phys. Rev. B* 89 (2014) 054409.
- [19] J.C. Wang, S. Aswartham, F. Ye, J. Terzic, H. Zheng, D. Haskel, S. Chikara, Y. Choi, P. Schlottmann, R. Custelcean, S.J. Yuan, G. Cao, Decoupling of the antiferromagnetic and insulating states in Tb-doped Sr_2IrO_4 , *Phys. Rev. B* 92 (2015) 214411.
- [20] Y. Klein, I. Terasaki, Insight on the electronic state of Sr_2IrO_4 revealed by cationic substitutions, *J. Phys.: Condens. Matter* 20 (2008) 295201.
- [21] J.M. Kong, S.L. Liu, J. Cheng, H.Y. Wang, X.A. Li, Z.H. Wang, Crystal structure and physical properties of the Sr-vacant spin-orbit-coupling induced Mott insulator $\text{Sr}_{2-x}\text{IrO}_4$, *Solid State Commun.* 220 (2015) 39.
- [22] Intiaz Noor Bhatti, R. Rawat, A. Banerjee, A.K. Pramanik, Temperature evolution of magnetic and transport behavior in 5d Mott insulator Sr_2IrO_4 : significance of magneto-structural coupling, *J. Phys.: Condens. Matter* 27 (2014) 016005.
- [23] J. Cheng, X.Y. Sun, S.L. Liu, B. Li, H.Y. Wang, P. Dong, Y. Wang, W. Xu, La-doping effect on spin-orbit coupled Sr_2IrO_4 probed by x-ray absorption spectroscopy, *New J. Phys.* 18 (2016) 093019.
- [24] E. Paris, B. Joseph, A. Iadecola, C. Marini, K. Kudo, D. Mitsuoka, M. Nohara, T. Mizokawa, N.L. Saini, Determination of temperature-dependent atomic displacements in the $\text{Ca}_{10}\text{Ir}_4\text{As}_8(\text{Fe}_2\text{As}_2)_5$ superconductor with a metallic spacer layer, *Phys. Rev. B* 90 (2014) 094508.
- [25] J. Cheng, P. Dong, W. Xu, S.L. Liu, W.S. Chu, X.H. Chen, Z.Y. Wu, Charge redistribution and a shortening of the Fe-As bond at the quantum critical point of $\text{SmO}_{1-x}\text{F}_x\text{FeAs}$, *J. Synchrotron Rad.* 22 (2015) 1030.
- [26] J.P. Clancy, N. Chen, C.Y. Kim, W.F. Chen, K.W. Plumb, B.C. Jeon, T.W. Noh, Y.J. Kim, Spin-orbit coupling in iridium-based 5d compounds probed by x-ray absorption spectroscopy, *Phys. Rev. B* 86 (2012) 195131.
- [27] X.Y. Sun, S.L. Liu, H.Y. Wang, B. Li, J. Cheng, Z.H. Wang, Insulator-metal transition in deep Sr-vacant spin-orbit Mott insulator Sr_2IrO_4 , *J. Alloy. Compd.* 687 (2016) 712.
- [28] M. Newville, IFEFFIT: interactive XAFS analysis and FEFF fitting, *J. Synchrotron Rad.* 8 (2001) 322.
- [29] The OPENMX (Open source package for Material eXplorer) software package for nanoscale material simulations, <http://www.openmx-square.org>.
- [30] T. Ozaki, Variationally optimized atomic orbitals for large-scale electronic structures, *Phys. Rev. B* 67(2003) 155108.
- [31] B.T. Thole, G. van der Laan, Branching ratio in x-ray absorption spectroscopy, *Phys. Rev. B* 38(1988) 3158.
- [32] G. van der Laan, B.T. Thole, Local Probe for Spin-Orbit Interaction, *Phys. Rev. Lett.* 60 (1988) 1977.
- [33] L.C. Chapon, S.W. Lovesey, The magnetic motif and the wavefunction of Kramers ions in strontium iridate Sr_2IrO_4 , *J. Phys.: Condens. Matter* 23 (2011) 252201.
- [34] M.A. Laguna-Marco, D. Haskel, N. Souza-Neto, J.C. Lang, V.V. Krishnamurthy, S. Chikara, G. Cao, M. van Veenendaal, Orbital Magnetism and Spin-Orbit Effects in the Electronic

Structure of BaIrO₃, Phys. Rev. Lett. 105 (2010) 216407.

- [35] J.S. Lee, Y. Krockenberger, K.S. Takahashi, M. Kawasaki, Y. Tokura, Insulator-metal transition driven by change of doping and spin-orbit interaction in Sr₂IrO₄, Phys. Rev. B 85 (2012) 035101.
- [36] J.J. Rehr, R.C. Albers, Theoretical approaches to x-ray absorption fine structure, Rev. Mod. Phys. 72 (2000) 621.
- [37] D.E. Sayers, B. Bunker, X-Ray Absorption: Principles, Applications, Techniques of EXAFS, SEXAFS, and XANES, New York, 1988.
- [38] A.L. Ankudinov, B. Ravel, J.J. Rehr, S.D. Conradson, Real-space multiple-scattering calculation and interpretation of x-ray-absorption near-edge structure. Phys. Rev. B 58 (1998) 7565.